Friction **10**(11): 1913–1926 (2022)
https://doi.org/10.1007/s40544-021-0581-6
ISSN 2223-7690
CN 10-1237/TH
RESEARCH ARTICLE

Design and characterization of metallic glass/graphene multilayer with excellent nanowear properties

Qing ZHOU[1], Dawei LUO[1], Dongpeng HUA[1], Wenting YE[1], Shuo LI[1,*], Qiguang ZOU[1], Ziqiang CHEN[2,3,*], Haifeng WANG[1,*]

[1] *State Key Laboratory of Solidification Processing, Center of Advanced Lubrication and Seal Materials, Northwestern Polytechnical University, Xi'an 710072, China*

[2] *Songshan Lake Materials Laboratory, Dongguan 523808, China*

[3] *Institute of Physics, Chinese Academy of Sciences, Beijing 100190, China*

Received: 29 June 2021 / Revised: 31 August 2021 / Accepted: 01 December 2021

Abstract: The excellent properties of metallic glass (MG) films make them perfect candidates for the use in miniature systems and tools. However, their high coefficients of friction (COFs) and poor wear resistance considerably limit their long-term performance in nanoscale contact. We report the fabrication of a MG/graphene multilayer by the repeated deposition of $Cu_{50}Zr_{50}$ MG with alternating layers of graphene. The microstructure of the multilayer was characterized by the transmission electron microscopy (TEM). Its mechanical and nanotribological properties were studied by nanoindentation and nanoscratch tests, respectively. A molecular dynamics (MD) simulation revealed that the addition of graphene endowed the MG with superelastic recovery, which reduced friction during nanoscratching. In comparison with the monolithic MG film, the multilayer exhibited improved wear resistance and a low COF in repeated nanowear tests owing to the enhanced mechanical properties and lubricating effect caused by the graphene layer. This work is expected to motivate the design of other novel MG films with excellent nanowear properties for engineering applications.

Keywords: metallic glass (MG); multilayer; nanowear properties; molecular dynamics (MD) simulation

1 Introduction

Metallic glass (MG) thin films have attracted much interest because of their smooth surfaces, thermoplastic forming ability, and excellent corrosion resistance [1–3]. Potential applications in nano-molds [4], micro-electro-mechanical systems [5], miniature parts [6], and medical tools such as microsurgery scissors [7] have been proposed. Friction and wear are highly important for these applications because they limit the device efficiency and lifetime [8–9]. Thus, considerable research on the surface tribological behavior of MG thin films has been performed to extend their applications [10].

According to the Archard equation, the wear resistance of materials is proportional to their hardness [11]. Monolithic MGs with high hardness are expected to have good wear resistance. However, the results to date often suggest that MGs have worse wear resistance than their nanocrystalline counterparts owing to the mechanical softening resulting from the rapid propagation of shear bands in MGs [12–16]. These shear bands can easily develop into microcracks, which form wear debris and result in poor wear resistance [17]. In addition, it is essential, but technically challenging, to reduce the coefficient of friction (COF) of MGs to improve the efficiency and reliability of mechanical systems [14, 18, 19]. The practical use of MG thin films

* Corresponding authors: Shuo LI, E-mail: shuoli2020@nwpu.edu.cn; Ziqiang CHEN, E-mail: chenziqiang@sslab.org.cn; Haifeng WANG, E-mail: haifengw81@nwpu.edu.cn

requires methods of reducing friction. However, few strategies have been provided to date despite their importance for safe application [3].

Great efforts have been made to improve the tribological properties of MGs, and increasing the toughness appears to be an effective method. Therefore, a glass-matrix composite with enhanced toughness has been developed by introducing a "soft" secondary phase [20]. However, the strength and hardness are unavoidably reduced by the formation of crystalline phases. By contrast, an efficient approach to achieving enhanced toughness and tribological properties is the use of bio-inspired laminated materials [21–25]. Films with designed multilayer architecture reportedly have superior mechanical and tribological properties compared to single monolithic films [26]. This result suggests that multilayers consisting of alternating layers of an MG and another high-strength material may exhibit better wear resistance.

Since its discovery in 2004, graphene has attracted much attention for the use in composite materials because of its exceptional properties. Specifically, the intrinsic breaking strength of graphene is 130 GPa [27], which suggests that it may improve both the strength and toughness of the multilayers when it is used as an interfacial reinforcement. More importantly, when it was applied as a typical two-dimensional (2D) material and an ideal solid lubricant phase [28], graphene reduced friction and wear [29–30]. Furthermore, the effects of a graphene layer on the friction and wear behaviors and the related mechanisms must be addressed. An in-depth understanding of the tribological properties and deformation mechanism of the MG/graphene multilayer is of great scientific interest and technological significance. The tribological properties of such advanced MG-based films have not yet been reported.

In this work, graphene grown by chemical vapor deposition (CVD) was introduced into a $Cu_{50}Zr_{50}$ MG to produce a laminated structure. The microstructure and mechanical properties of the structure were explored. Continuous improvements in the machining of MG thin films at nanoscale, that is, approaching nanoscratching [31–33], can provide insights into the friction, wear, and chip-separation behavior. Accordingly, the nano/micro-tribological performance of the MG films was thoroughly investigated by the nanoscratch technique, and the corresponding wear mechanisms were studied. These results could offer a promising approach to improving the wear resistance of the MG films.

2 Experimental

2.1 Fabrication of MG/graphene multilayered composites

As illustrated in Fig. 1, a multilayer consisting of alternating layers of 150 nm thick $Cu_{50}Zr_{50}$ MG and graphene was prepared.

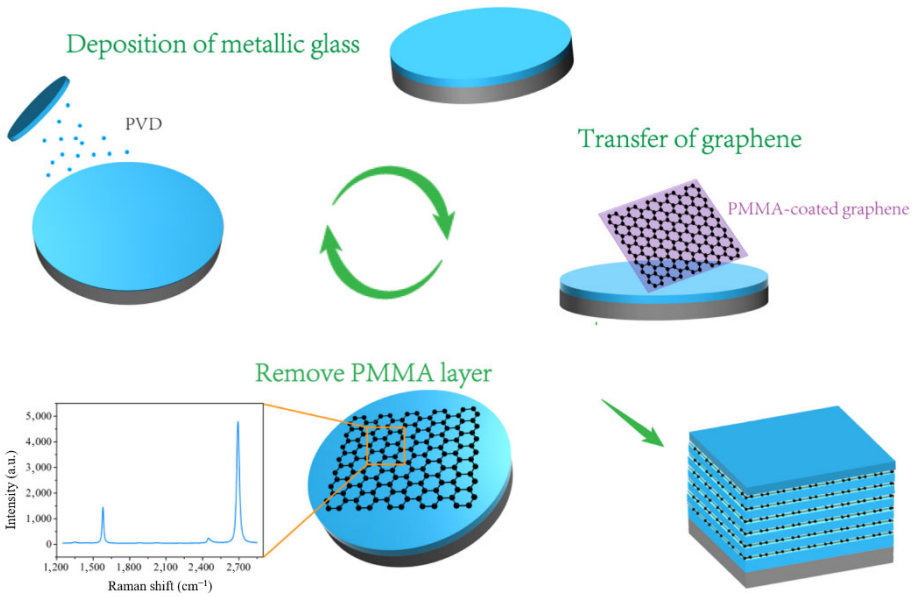

Fig. 1 Schematic diagram of the fabrication of the multilayer with alternating layers of $Cu_{50}Zr_{50}$ MG and graphene.

1) A thick MG seed layer was deposited on a silicon wafer by physical vapor deposition (PVD) using an amorphous $Cu_{50}Zr_{50}$ target [3]. The chemical composition of the $Cu_{50}Zr_{50}$ MG was examined by the energy dispersive X-ray spectroscopy (EDS), and its amorphous nature was confirmed by the transmission electron microscopy (TEM).

2) Graphene films were synthesized by CVD on a commercially available copper foil, which was ultrasonically cleaned sequentially with deionized H_2O, acetone, and ethyl alcohol before the graphene growth. The obtained graphene was spin coated with polymethyl methacrylate (PMMA) to form a support layer [34].

3) The obtained graphene/PMMA films were etched with HCl and transferred to the surface of the deposited MG film, and acetone was used to remove the PMMA layer. The Raman spectrum of the surface shows strong symmetric 2D and G peaks but no D peak, as shown in the inset of Fig. 1, indicating that the transferred graphene is of high quality (defect-free) [35].

4) MG film deposition and graphene transfer were conducted alternately to produce an MG/graphene multilayered composite. The topmost layer was MG, and the total thickness was 1.2 μm. For comparison, a monolithic MG film was also prepared by the same process (including the washing step) but without incorporating graphene.

2.2 Characterization of microstructure and mechanical properties

The cross-sectional morphology of the MG/graphene multilayer was obtained by the focused ion beam lithography and TEM (Talos F200X G2, FEI, USA). The nano-indenter system (XP, MTS, USA) operating in continuous stiffness measurement mode [36–39] was employed to characterize the hardness of the monolithic $Cu_{50}Zr_{50}$ MG and MG/graphene films. For the continuous measurement of the modulus (E) and hardness (H) during indentation, the diamond tips were exposed to a weak oscillation (frequency (f) = 45 Hz, amplitude (Δh) = 2 nm). Calibration on synthetic fused silica revealed that the indenter tip radius was ~50 nm. The E and H values of the samples were obtained using a depth control mode (strain rate = 0.05 s^{-1}). The preset depth was 200 nm to ensure that the indentation process affected the graphene layer. The E and H values of each sample were averaged from 16 tests.

2.3 Nanowear tests

Nanoscratch tests were performed in both ambient and dry atmosphere employing a Hysitron Triboindenter system (TI980, Hysitron, USA). To avoid the effects of tip geometry, a cono- spherical diamond tip with a cone angle and effective radius of π/2 and ~1 μm, respectively, was used. Nanoscratch tests were conducted at a speed and constant load of 1 μm·s^{-1} and 5 mN, respectively (frictional heating did not significantly increase the local temperature [40]). The scratched surfaces were then examined by a built-in scanning probe microscope (TI980, Hysitron, USA). In addition, repeated nanoscratching at the same position was performed eight times in this nanowear experiment. All of these scratch tests were repeated more than three times on each sample (usually four times) with parallel tracks separated by 100 μm. After the tests, the scratch track and pit morphology were also examined by the field emission scanning electron microscope (SEM; Gemini SEM 500, Carl Zeiss, Germany). The EDS (Ultradry, Thermo Scientific, USA) with an accelerating voltage of 10 kV and a working distance of 10 mm was used to determine the chemical composition of the worn grooves.

3 Computation

To explore the friction mechanisms, the nanoscratching behaviors of both specimens were investigated by a molecular dynamics (MD) simulation using a large-scale atomic/molecular massively parallel simulator [41]. The atomic interactions among metallic atoms and carbon atoms were obtained using the embedded atom method potential [42] and the adaptive intermolecular reactive bond order potential [43], respectively. Additionally, the atomic interactions among metallic atoms and carbon atoms were obtained using the Lennard–Jones potential, where the related parameters were the same as those in Ref. [44].

To build the atomic-scale models of the multilayer, we began with a small $Cu_{50}Zr_{50}$ MG with dimensions of 5 nm × 5 nm × 5 nm. The alloy was melted at 2,300 K and subsequently cooled to 300 K at a rate of

5×10^{12} K·s^{-1}. During this process, the isothrmal–isobaric (NPT) ensemble and three-dimensional periodic boundary conditions were applied, and the time step was 2 fs. This $Cu_{50}Zr_{50}$ model was then replicated, annealed at 800 K for 500 ps, and cooled to 300 K to produce a large MG model, as shown in Fig. 2(a). The structure of graphene is shown in Fig. 2(b), where the in-plane size is the same as that of the MG model, and the thickness is 0.335 nm [45]. Finally, the MG layer and graphene sheet were deposited alternately to form the multilayer. Because of limited computational efficiency, the MG layer thickness was scaled to 1.5 nm, and the size of the multilayer in the z direction was thus 12.1 nm to ensure that six graphene layers were interspersed between seven MG layers. Consequently, the qualitative features of our simulation reproduce the experimental conditions well. Figure 2(c) shows a schematic of the multilayer and the configuration parameters.

The simulation of scratching deformation had two stages: nanoindentation and nanoscratching. The indenter first indented the material along the z direction until the load reached 0.2 μN, and then moved along the x direction (zigzag direction of graphene layer). To eliminate the possible effect of the orientation of the graphene layer on the tribological behavior, an identical scratching process along the y direction (armchair direction of graphene layer) was also conducted (Fig. S1 in the Electronic Supplementary Material (ESM)). When scratching was performed along the armchair direction, the effects of graphene on the tribological properties, elastic behavior, and plastic behavior were identical to those observed when scratching was performed along the zigzag direction, indicating that the graphene layer orientation had a negligible effect (Fig. S2 in the ESM). Thus, for simplicity, the simulation results of scratching in the zigzag direction are shown as representative results hereafter. The simulated scratching speed was 20 m·s^{-1}, which is much higher than that in the experiment. If a speed on the order of micrometers per second is used in the simulation, the time required for the calculation is at least 7 orders of magnitude higher [46]. In this simulation, the chosen parameters did not qualitatively change any trend in the tribological response and deformation mechanism, and comparisons of absolute values between experiments and simulations are meaningless [46]. In the above scratching process, we used the fixed boundary on the sides to prevent the model from moving. Before loading, the sample was relaxed for 10 ps at 300 K to release the excess energy.

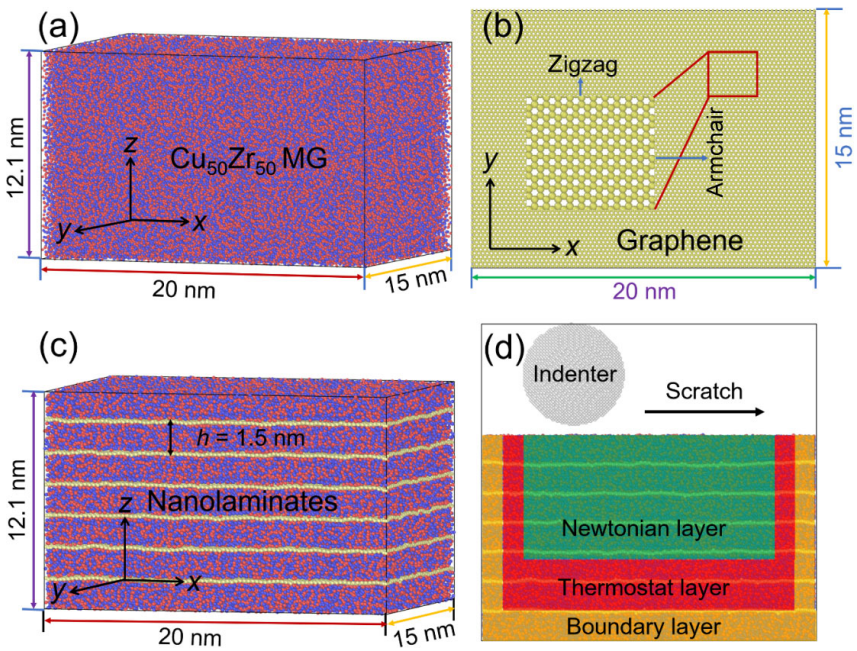

Fig. 2 Initial atomic configurations of (a) monolithic $Cu_{50}Zr_{50}$ MG, (b) graphene, and (c) $Cu_{50}Zr_{50}$ MG/graphene multilayer. The MG layer thickness is denoted as h in (c). (d) MD simulation model of nanoscratching.

4 Results and discussion

4.1 Microstructure and mechanical properties

Figure 3(a) shows the TEM images of the microstructure of the MG/graphene composite. The interfacial graphene layers can be identified clearly in the TEM bright-field image. Figure 3(b) shows high-angle annular dark-field (HAADF) image of the MG/graphene multilayer, which reveals the laminated structure. The measured individual layer thickness of the multilayer MG/graphene film was 204.51±22.06 nm. The mechanical characterization of the monolithic MG film and MG/graphene was performed by depth-resolved indentation tests. Representative depth profiles of the obtained hardness and elastic modulus of both samples are shown in Fig. 4. A remarkable indentation size effect (ISE) was identified; that is, when the indenter displacement increased, the hardness and modulus values decreased. The ISE is particularly pronounced when the indentation depth is shallow, and the hardness and modulus values each approach a constant value when the displacement depth exceeds a certain threshold. The origin of the ISE in MGs is generally regarded as strain-induced softening resulting from the continuous creation and coalescence of free volumes upon indentation [36, 47]. Because the number of additional free volumes that form is proportional to the total strain, MGs are likely to become progressively softer during the initial indentation process, resulting in an ISE. In addition to the depth dependence of the mechanical properties, the H and E values of the multilayer clearly increased. H increased from 6.7 GPa for the monolithic MG to 7.8 GPa for the multilayer. Here, to avoid the ISE and substrate effects, the intrinsic hardness values were determined by calculating the mean values in a specific depth range (1/10 to 1/7 of the film thickness) in which a plateau is reached [48]. Similarly, E increased from 124 GPa for the monolithic MG to 138 GPa for the multilayer.

To clarify the strengthening effect of the graphene

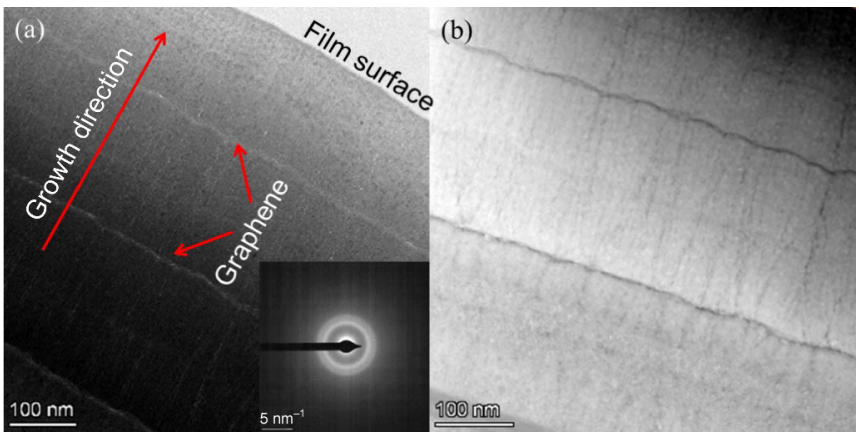

Fig. 3 (a) Cross-sectional TEM image of MG/graphene multilayer. Growth direction and graphene layer are marked. (b) HAADF image of MG/graphene sample showing the laminated structure.

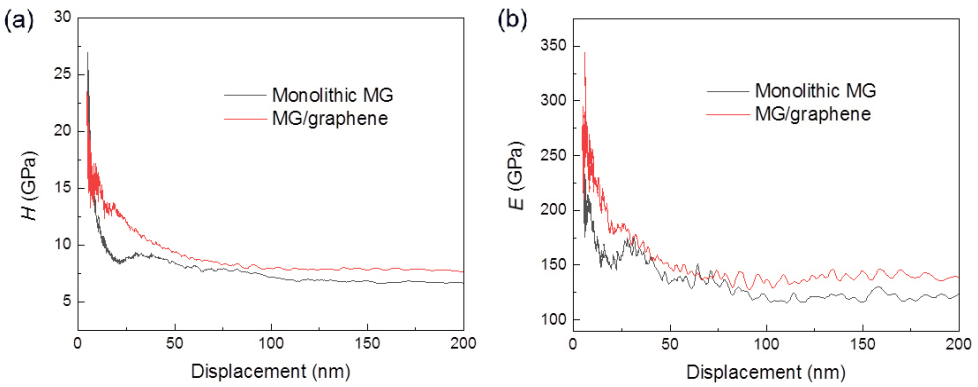

Fig. 4 Depth profiles of (a) H and (b) E of the monolithic MG film and MG/graphene multilayer as determined by nanoindentation tests.

interface, the deformation behavior of the monolithic $Cu_{50}Zr_{50}$ MG and MG/graphene multilayer films is shown in Fig. 5. As shown in Fig. 5(a), shear bands in the monolithic MG, which appeared as the aggregation of shear atoms, were nucleated from the severely deformed region beneath the indenter and propagated freely downward (as indicated by white arrows). By contrast, shear banding around the indenter in the MG/graphene multilayer was effectively blocked by the graphene interfaces, as shown in Fig. 5(b), improving the hardness of the multilayer [49].

4.2 Tribological performance

4.2.1 Friction force

To illustrate the nanoscratching process, the normal force and lateral displacement as a function of time are plotted in Fig. 6(a). The procedure involved three sequential scratches:

1) Pre-scratch: The surface was scanned at 2 μN to obtain the slope and roughness of the surface (pure elastic deformation without wear occurs in this process).

2) On-load scratch: The tip scratched the films at the preset load.

3) Post-scratch: The surface was scanned at 2 μN to obtain the residual depth.

The scratch data were analyzed by leveling the sample slope and subtracting the frame compliance to obtain a true depth profile under the applied load and during the topography measurements [50]. Figure 6(b) shows a plot of scratch depth vs. lateral displacement for the monolithic MG as an example. The indenter displacements during on-load scratching indicate the elastic and plastic deformation. The indenter displacements during post-scratching reflect the residual wear depth. The difference between these two depths simply demonstrates the elastic recovery of the material after scratching.

Figure 7(a) shows the lateral forces on the indenter as it scratched the two films as a function of displacement. After the unstable run-in stage [2], the lateral force reached a steady-state value for both samples. In addition, the friction force was lower in the multilayer than that in the monolithic MG, indicating that the graphene layer has a lubricating

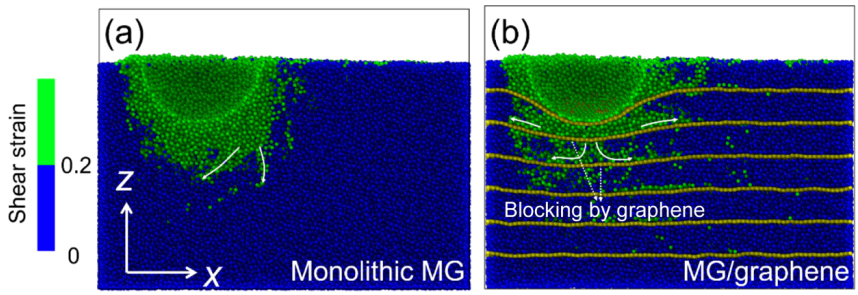

Fig. 5 Shear Von Mises strain distributions of (a) monolithic $Cu_{50}Zr_{50}$ MG and (b) MG/graphene multilayer upon deformation. Atoms are colored according to the value of the shear Von Mises strain (η_i^{Mises}), where green atoms represent shear atoms with $\eta_i^{\text{Mises}} \geq 0.2$, and blue atoms represent those with $\eta_i^{\text{Mises}} < 0.2$.

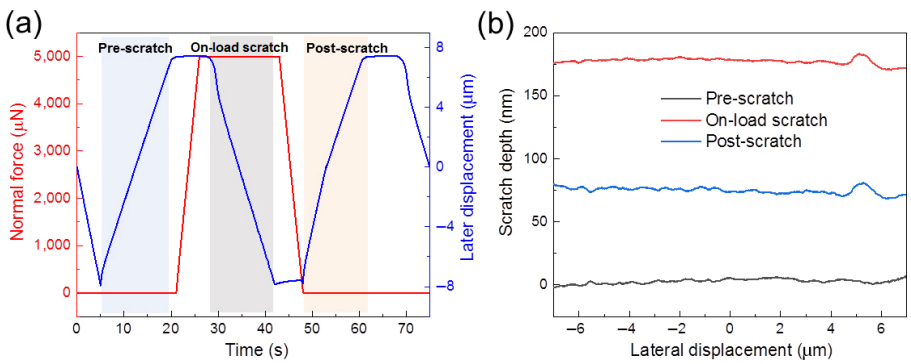

Fig. 6 (a) Representative profile of nanoscratching process. (b) Representative scratch depth profile of $Cu_{50}Zr_{50}$ MG as a function of lateral displacement.

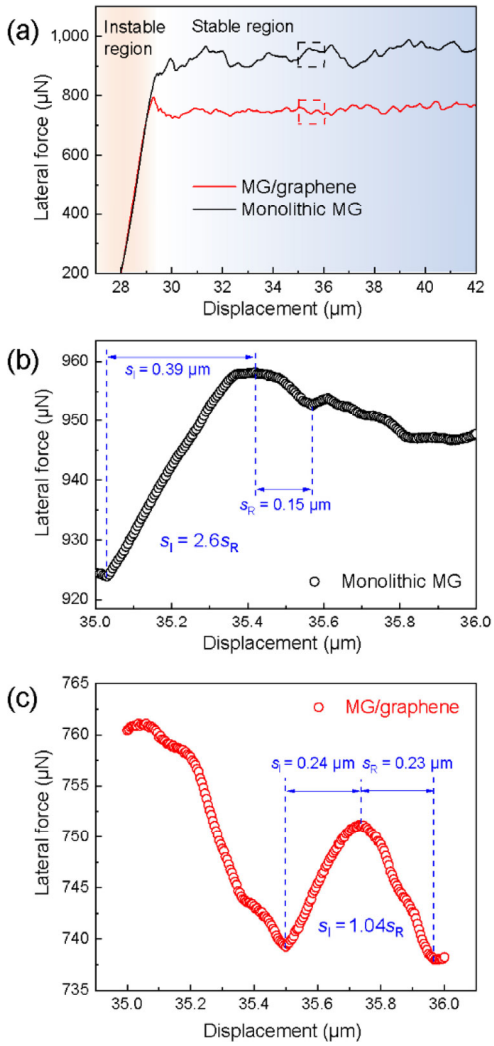

Fig. 7 (a) Lateral force as a function of displacement for the two films. Enlarged lateral force–displacement curves of (b) monolithic MG and (c) MG/graphene multilayer within the dotted rectangles in (a).

effect. Another observation is that the varying lateral force included several serration events, which are identified as the stick–slip behavior caused by the nucleation and propagation of shear bands during scratching [51–53]. Intuitively, the fluctuation of the serrations is smaller in the multilayer than that in the monolithic MG, suggesting more pronounced shear band nucleation and shear band–interface interactions in the MG/graphene multilayer, as discussed below.

The serration events are shown in more detail in the enlarged curves in Figs. 7(b) and 7(c), which show that the stick–slip behavior involves both processes that increase and relax the force. During the process that increases the force, structural strengthening facilitates the accommodation of the plastic strain [3]. After reaching a maximum value, the force decreases, resulting in the shear separation of the sample surfaces, and materials accumulate around the groove [54–55]. The force accumulation displacement (s_I) and relaxation displacement (s_R) are marked in Figs. 7(b) and 7(c). The ratio of s_I/s_R for the monolithic MG is much larger than that for the multilayer.

To investigate the effect of graphene on the scratching deformation, MD simulations were performed to shed light on the corresponding mechanism, as shown in Fig. 8. The atoms with a shear Von Mises strain of $\eta_i^{\text{Mises}} \geq 0.2$ were defined as shear atoms and employed to visualize the local plastic events in the film [56]. The region with a high density of shear atoms was identified as the shear deformation region (SDR), which consists of the crossed and stacked shear bands around the indenter [57]. Figures 8(a) and 8(b) show the shear Von Mises strain distributions of the monolithic $Cu_{50}Zr_{50}$ and MG/graphene multilayer during nanoscratching along the x direction. Like that during the nanoindentation tests, the SDR expansion during nanoscratching is strongly blocked by the graphene interface, as shown by the arrow in Fig. 8(b). Ahead of the SDR, an embryonic shear band developed from the interface, as indicated by the ellipse. Because the atomic packing density of the MG at the interface is always lower than those of the atoms inside the layer, excess free volumes are therefore promoted in the interface region [57–58]. However, the presence of the graphene layer causes a complex stress concentration at the interface, which positively affects shear band nucleation [57].

The simulation results indicate that the graphene layer functions as a source and barrier for shear deformation during nanoscratching. Therefore, numerous shear banding processes can be activated, and little shear fluctuation is observed in the multilayer because of the intensive shear band–interface interactions. This finding can explain why the serrations in the multilayer are more numerous and smaller in amplitude than those in the monolithic MG (Fig. 7). In the monolithic MG, s_I is much larger than that of s_R. This result indicates a rapid decrease in serration events in the monolithic MG. By contrast, the smaller value of s_I/s_R suggests that the force

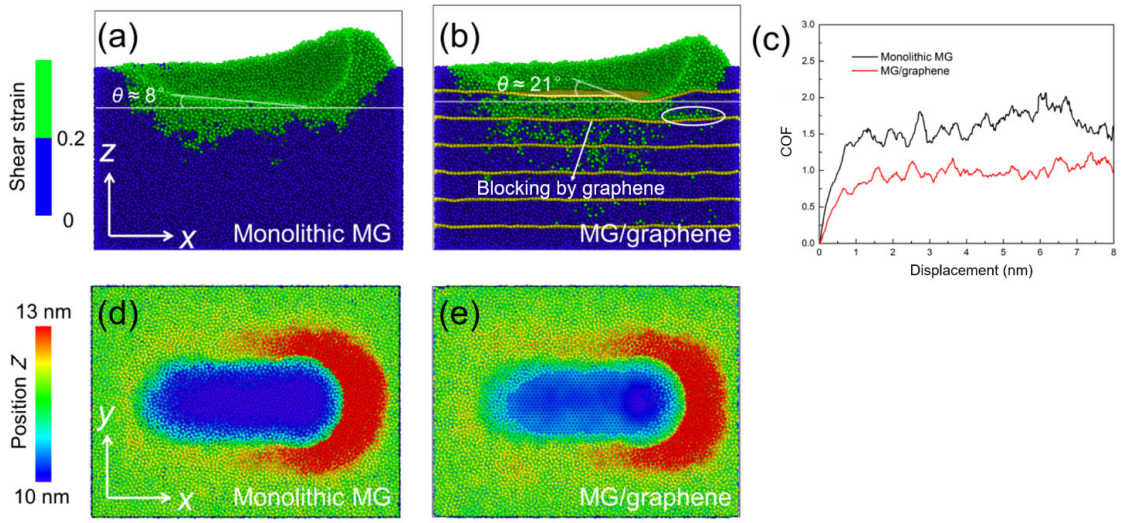

Fig. 8 Shear Von Mises strain distributions of (a) monolithic $Cu_{50}Zr_{50}$ MG and (b) MG/graphene multilayer during nanoscratching. Atoms are colored according to the value of the shear Von Mises strain, where green atoms represent shear atoms with $\eta_i^{\text{Mises}} \geq 0.2$, and blue atoms represent those with $\eta_i^{\text{Mises}} < 0.2$. (c) Friction force of each sample as a function of sliding displacement. Surface morphologies of (d) monolithic $Cu_{50}Zr_{50}$ MG and (e) MG/graphene multilayer.

relaxation process is prolonged in the serration events in the multilayer. Because graphene limits deformation, the forces that accumulate in each serration event are not completely released within a short period of time. This behavior results in an incomplete plastic relaxation and a decrease in the serration amplitude owing to the presence of graphene. Consequently, the relaxation time approaches the reloading time, which favors the formation of the new shear bands at interfaces. In particular, the multilayer exhibits unique hardening behavior under the condition for the coexistence of numerous shear bands and the interface. Thus, the introduction of graphene layers increases the H value of the multilayer.

The COF is also lower in the multilayer than that in the monolithic MG, as shown in Figs. 7 and 8(c). Cross-sectional views of the two samples clearly show the elastic recovery (or rebound) behind the indenter [46], resulting in an inclined groove surface, as shown in Figs. 8(a) and 8(b). Note that the residual depth of the multilayer recovers more quickly, resulting in a more slanted surface at the rear of the indentation. To quantify the rebound ability, the slope angle (θ) of the scratched groove was measured. We found that the θ value of the multilayer is much larger than that of the monolithic MG, which is related to the strong elastic recovery and large modulus of graphene. Indeed, previous studies have shown that the elastic recovery could significantly affect friction [59–61], and thus a higher elastic recovery can result in a smaller plowing friction [40]. In sum, the presence of the graphene layer can contribute to a simultaneous improvement in the elastic recovery and hardness. Therefore, a smaller COF in the multilayer seems plausible.

4.2.2 *Wear depth*

Figure 9(a) shows a plot of scratch depth vs. lateral displacement. The $Cu_{50}Zr_{50}$ MG has a larger wear depth (post-scratch) than that of the multilayer, suggesting that the multilayer has better scratch resistance. This property is attributed in part to the graphene strengthening effect discussed above. In addition, Fig. 9(b) shows that the multilayer exhibits dramatically improved elastic recovery after scratching, which contributes significantly to the wear resistance of the MG/graphene multilayer. This result is also in agreement with the MD prediction as shown in Figs. 8(a) and 8(b).

Figure 10 shows the cross-sectional profiles of the grooves after scratching. All the nanoscratches display the same features (i.e., a groove with clear side-flow and material accumulation on the lateral sides), indicating ductile plowing wear in the films [62]. The surface height profiles as shown in Fig. 10(c) also show that both the height of the accumulated material and

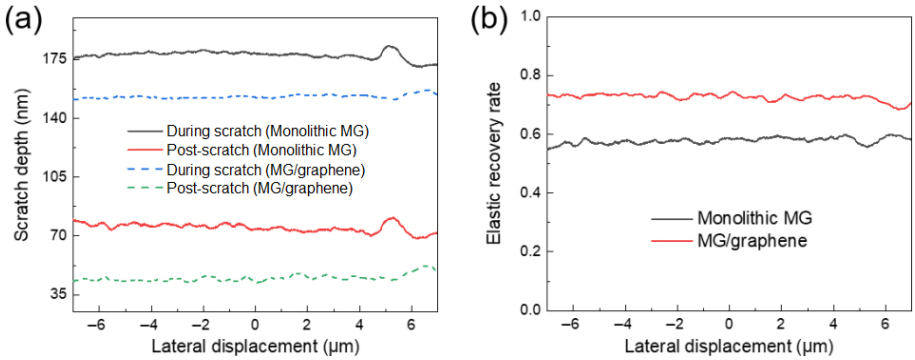

Fig. 9 (a) Scratch depth and (b) elastic recovery profiles of two films as a function of lateral displacement.

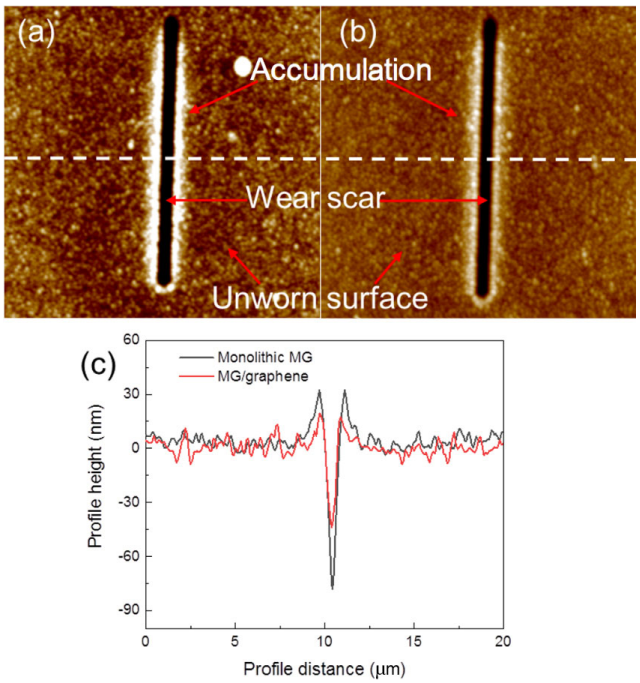

Fig. 10 Surface topographies of (a) monolithic $Cu_{50}Zr_{50}$ MG and (b) MG/graphene multilayer after nanoscratching at a load of 5 mN. (c) Surface height profiles of each sample along the dotted line in (a) and (b).

wear depth are lower in the multilayer, indicating lower material loss and higher wear resistance compared to the monolithic MG.

Next, up to eight test cycles under a load of 5 mN were performed on the two samples to explore the nanowear properties. The wear resistance was explored by calculating the material volume removed by scratching (V), which was calculated as Eq. (1) [3, 63]:

$$V = \int_0^x h_x^2 \tan\alpha \mathrm{d}x \quad (1)$$

where x denotes the length of a scratch, h_x indicates the depth of the scratch at x, and α represents the half-cone angle of the indenter. Then the wear rate was measured as the ratio of wear volume to cycle number [64]. Figure 11(a) demonstrates that for the multilayer, the wear rate first decreases, and then steady-state wear is observed after five cycles. More importantly, the wear rate of the multilayer is much lower than that of the monolithic MG.

The variation of the COF with wear cycle is shown in Fig. 11(b). The decrease in friction during the initial wear cycles is related to a reduction in plowing depth, as reported previously [65]. However, the COF of the monolithic MG then starts to increase with increasing number of wear cycles. By contrast, a significant decrease in friction is observed in the multilayer, indicating a more stable wear process throughout the test. The typical surface topographies of the two samples are shown in Figs. 11(c) and 11(d). After multiple scratches, plastic deformation in the monolithic MG is followed by partial crack and fracture at the edge of the wear track, as indicated in Fig. 11(c). By contrast, the multilayer has a much smoother surface (Fig. 11(d)) and shows no sign of crack after eight wear cycles. The promotion of plasticity at the interfaces and the suppression of shear band propagation by graphene endow the multilayer with excellent homogeneous deformation ability during repeated sliding. This improved toughness results in better wear resistance. More importantly, some carbon is present on the scratch grooves of the multilayer, as indicated by the EDS analysis (Table 1, Fig. S3, and Table S1 in the ESM). With the gradual wearing of the top MG layer, graphene plays a more important role in reducing the sliding resistance at the contact surface owing to its weak interaction with the

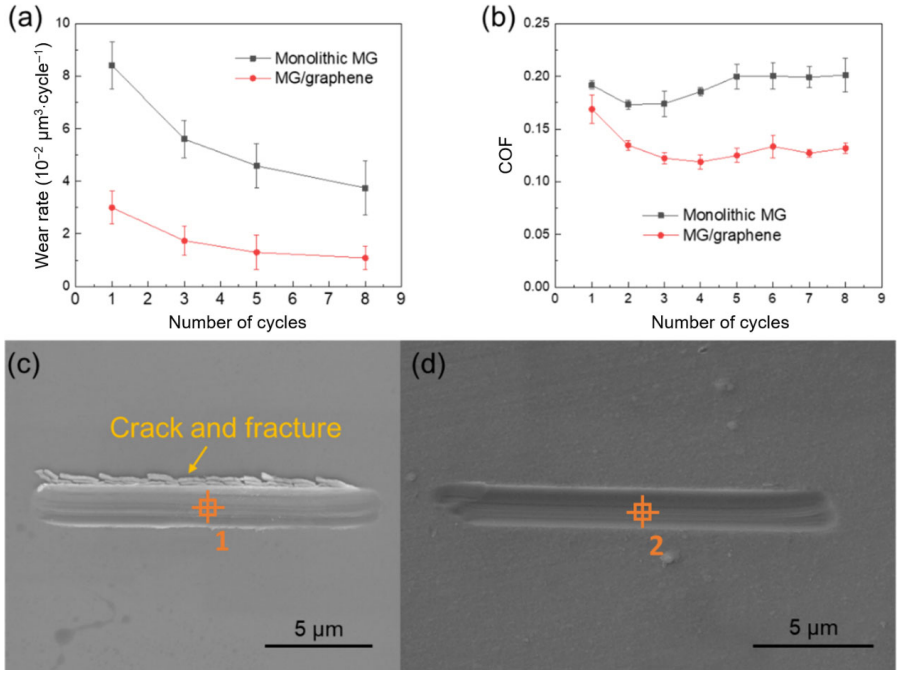

Fig. 11 Variations of (a) wear rate and (b) COF as a function of wear cycle for monolithic $Cu_{50}Zr_{50}$ MG and MG/graphene multilayer. SEM images of worn grooves in (c) monolithic $Cu_{50}Zr_{50}$ MG and (d) MG/graphene multilayer. SEM observation at the periphery of the wear scar shows the formation of the microcracks and the fracture of the materials along the scratch groove, indicating the brittle nature of the monolithic MG. By contrast, the multilayer shows a much smoother surface without crack or delamination, indicating the lubricating effect of graphene. EDS analyses of Regions labeled 1 and 2 are shown in Table 1.

Table 1 Elemental composition (at%) from EDS analysis in Fig. 11.

	Cu	Zr	C	O
1	42.27±0.83	34.52±1.35	—	23.21±1.07
2	44.87±0.80	35.77±1.27	6.74±0.51	12.62±0.92

indenter [66]. The CVD-grown graphene, which exhibited strong potential for effectively reducing the nanoscale adhesion and friction as an atomically thin solid lubricant [67], can protect the surface from further damage and wear. By contrast, the monolithic MG was more brittle under cyclic loading, which resulted in higher friction and wear at the end of the test. In summary, the wear resistance can be dramatically enhanced by introducing graphene to provide higher toughness and self-lubricating ability.

5 Conclusions

An MG/graphene composite film with a laminated structure was prepared by a combination of PVD and CVD. The mechanical and tribological properties of the multilayer were investigated by nanoindentation and nanoscratch tests, respectively. The hardness and elastic modulus of the multilayer increased by 16.7% and 11%, respectively, compared with those of the monolithic MG film owing to the high strength and elastic modulus of graphene. In particular, the nanoscratch results indicate that the introduction of graphene significantly reduced friction and wear. An MD simulation revealed that graphene endows MG with superelastic recovery ability, which reduces the sliding friction. In repeated nanowear tests, graphene played a crucial role in enhancing the wear resistance of the multilayer owing to its higher homogeneous deformation ability and damage tolerance. In addition, its self-lubricating effect appeared in the continuous wear process, resulting in a lower COF and good wear performance compared with the monolithic MG film. These results suggested that the design of

alternately layered MG/graphene multilayer is effective for enhancing the nanowear properties for engineering applications.

Acknowledgements

The authors would like to thank the National Natural Science Foundation of China (No. 51801161); Guangdong Basic and Applied Basic Research Foundation, China (No. 2021A1515010756); the Natural Science Foundation of Jiangsu Province, China (No. BK20180266); and the Fundamental Research Funds for the Central Universities (No. 3102019JC001).

Electronic Supplementary Material Supplementary material is available in the online version of this article at https://doi.org/10.1007/s40544-021-0581-6.

References

[1] Diyatmika W, Chu J P, Kacha B T, Yu C C, Lee C M. Thin film metallic glasses in optoelectronic, magnetic, and electronic applications: A recent update. *Curr Opin Solid State Mater Sci* **19**(2): 95–106 (2015)

[2] Chu J P, Jang J S C, Huang J C, Chou H S, Yang Y, Ye J C, Wang Y C, Lee J W, Liu F X, Liaw P K, et al. Thin film metallic glasses: Unique properties and potential applications. *Thin Solid Films* **520**(16): 5097–5122 (2012)

[3] Zhou Q, Du Y, Ren Y, Kuang W W, Han W C, Wang H F, Huang P, Wang F, Wang J. Investigation into nanoscratching mechanical performance of metallic glass multilayers with improved nano-tribological properties. *J Alloys Compd* **776**: 447–459 (2019)

[4] Kobata J, Miura K, Amiya K, Fukuda Y, Saotome Y. Nanoimprinting of Ti–Cu-based thin-film metallic glasses deposited by unbalanced magnetron sputtering. *J Alloys Compd* **707**: 132–136 (2017)

[5] Sambandam S N, Bhansali S, Bhethanabotla V R. Synthesis and characterization of amorphous metallic alloy thin films for MEMS applications. *Mater Res Soc Symp Proc* **806**: 177–182 (2003)

[6] Schroers J. Processing of bulk metallic glass. *Adv Mater* **22**(14): 1566–1597 (2010).

[7] Tsai P H, Li T H, Hsu K T, Chiou J W, Jang J S C, Chu J P. Effect of coating thickness on the cutting sharpness and durability of Zr-based metallic glass thin film coated surgical blades. *Thin Solid Films* **618**: 36–41 (2016)

[8] Meng Y G, Xu J, Jin Z M, Prakash B, Hu Y Z. A review of recent advances in tribology. *Friction* **8**(2): 221–300 (2020)

[9] Yan J F, Lindo A, Schwaiger R, Hodge A M. Sliding wear behavior of fully nanotwinned Cu alloys. *Friction* **7**(3): 260–267 (2019)

[10] Han D X, Wang G, Li J, Chan K C, To S, Wu F F, Gao Y L, Zhai Q J. Cutting characteristics of Zr-based bulk metallic glass. *J Mater Sci Technol* **31**(2): 153–158 (2015)

[11] Archard J F. Contact and rubbing of flat surfaces. *J Appl Phys* **24**(8): 981–988 (1953)

[12] Morris D G. A study of the wear behaviour of amorphous and crystallised metallic alloys. In: *Rapidly Quenched Metals II*. Steeb S, Warlimont H, Eds. Amsterdam (the Netherlands): Elsevier Science Publishers, 1985: 1775–1778.

[13] Wu C D. Molecular dynamics simulation of nanotribology properties of CuZr metallic glasses. *Appl Phys A* **122**(4): 486 (2016)

[14] Wang J G, Choi B W, Nieh T G, Liu C T. Nano-scratch behavior of a bulk Zr–10Al–5Ti–17.9Cu–14.6Ni amorphous alloy. *J Mater Res* **15**(4): 913–922 (2000)

[15] Branagan D J, Swank W D, Haggard D C, Fincke J R. Wear-resistant amorphous and nanocomposite steel coatings. *Metall Mater Trans A* **32**(10): 2615–2621 (2001)

[16] Jin H W, Ayer R, Koo J Y, Raghavan R, Ramamurty U. Reciprocating wear mechanisms in a Zr-based bulk metallic glass. *J Mater Res* **22**(2): 264–273 (2007)

[17] Zhou Q, Han W C, Du Y, Wu H X, Bird A, Zhao X X, Wang X Z, Wang H F, Beake B D. Enhancing fatigue wear resistance of a bulk metallic glass via introducing phase separation: A micro-impact test analysis. *Wear* **436–437**: 203037 (2019)

[18] Kang S J, Rittgen K T, Kwan S G, Park H W, Bennewitz R, Caron A. Importance of surface oxide for the tribology of a Zr-based metallic glass. *Friction* **5**(1): 115–122 (2017)

[19] Fleury E, Lee S M, Ahn H S, Kim W T, Kim D H. Tribological properties of bulk metallic glasses. *Mater Sci Eng A* **375–377**: 276–279 (2004)

[20] Zhou Q, Ren Y, Du Y, Han W C, Hua D P, Zhai H M, Huang P, Wang F, Wang H F. Identifying the significance of Sn addition on the tribological performance of Ti-based bulk metallic glass composites. *J Alloys Compd* **780**: 671–679 (2019)

[21] Economy D R, Mara N A, Schoeppner R L, Schultz B M, Unocic R R, Kennedy M S. Identifying deformation and strain hardening behaviors of nanoscale metallic multilayers through nano-wear testing. *Metall Mater Trans A* **47**(3): 1083–1095 (2016)

[22] Cao Y Z, Zhang J J, Liang Y C, Yu F L, Sun T. Mechanical and tribological properties of Ni/Al multilayers—A molecular dynamics study. *Appl Surf Sci* **257**(3): 847–851 (2010)

[23] Topić M, Favaro G, Bucher R. Scratch resistance of platinum–vanadium single and multilayer systems. *Surf Coat Technol* **205**(20): 4784–4790 (2011)

[24] Beake B D, Ranganathan N. An investigation of the nanoindentation and nano/micro-tribological behaviour of monolayer, bilayer and trilayer coatings on cemented carbide. *Mater Sci Eng A* **423**(1–2): 46–51 (2006)

[25] Khadem M, Penkov O V, Yang H K, Kim D E. Tribology of multilayer coatings for wear reduction: A review. *Friction* **5**(3): 248–262 (2017)

[26] Zhang C, Zhang B S, Xie L S. Improving mechanical properties of Ni–W based nanocrystalline films by multilayered architecture. *Surf Coat Technol* **402**: 126341 (2020)

[27] Lee C, Wei X, Kysar J W, Hone J. Measurement of the elastic properties and intrinsic strength of monolayer graphene. *Science* **321**(5887): 385–388 (2008)

[28] Zhang C, Yang B Q, Wang J, Wang H F, Liu G, Zhang B S, Liu L J, Feng K, Li Z G. Microstructure and friction behavior of LaF_3 doped Ti-MoS_2 composite thin films deposited by unbalanced magnetron sputtering. *Surf Coat Technol* **359**: 334–341 (2019)

[29] Liu L C, Zhou M, Jin L, Li L C, Mo Y T, Su G S, Li X, Zhu H W, Tian Y. Recent advances in friction and lubrication of graphene and other 2D materials: Mechanisms and applications. *Friction* **7**(3): 199–216 (2019)

[30] Ji Z J, Zhang L, Xie G X, Xu W H, Guo D, Luo J B, Prakash B. Mechanical and tribological properties of nanocomposites incorporated with two-dimensional materials. *Friction* **8**(5): 813–846 (2020)

[31] Beake B D, Vishnyakov V M, Harris A J. Nano-scratch testing of (Ti,Fe)N_x thin films on silicon. *Surf Coat Technol* **309**: 671–679 (2017)

[32] Chowdhury S, Polychronopoulou K, Cloud A, Abelson J R, Polycarpou A A. Nanomechanical and nanotribological behaviors of hafnium boride thin films. *Thin Solid Films* **595**: 84–91 (2015)

[33] He W J, Zeng Q F. Enhanced micro/nano-tribological performance in partially crystallized 60NiTi film. *Friction* **9**(6): 1635–1647 (2021)

[34] Li X, Cai W, An J, Kim S, Nah J, Yang D, Piner R, Velamakanni A, Jung I, Tutuc E, et al. Large-area synthesis of high-quality and uniform graphene films on copper foils. *Science* **324**(5932): 1312–1314 (2009)

[35] Lei Y, Jiang J L, Bi T T, Du J F, Pang X J. Tribological behavior of *in situ* fabricated graphene–nickel matrix composites. *RSC Adv* **8**(39): 22113–22121 (2018)

[36] Limbach R, Kosiba K, Pauly S, Kühn U, Wondraczek L. Serrated flow of CuZr-based bulk metallic glasses probed by nanoindentation: Role of the activation barrier, size and distribution of shear transformation zones. *J Non Cryst Solids* **459**: 130–141 (2017)

[37] Du Y, Zhou Q, Jia Q, Shi Y D, Wang H F, Wang J. Imparities of shear avalanches dynamic evolution in a metallic glass. *Mater Res Lett* **8**(10): 357–363 (2020)

[38] Hua D P, Xia Q S, Wang W, Zhou Q, Li S, Qian D, Shi J Q, Wang H F. Atomistic insights into the deformation mechanism of a CoCrNi medium entropy alloy under nanoindentation. *Int J Plast* **142**: 102997 (2021)

[39] Zhou Q, Han W C, Luo D W, Du Y, Xie J Y, Wang X Z, Zou Q G, Zhao X X, Wang H F, Beake B D. Mechanical and tribological properties of Zr–Cu–Ni–Al bulk metallic glasses with dual-phase structure. *Wear* **474–475**: 203880 (2021)

[40] Ye Y X, Liu C Z, Wang H, Nieh T G. Friction and wear behavior of a single-phase equiatomic TiZrHfNb high-entropy alloy studied using a nanoscratch technique. *Acta Mater* **147**: 78–89 (2018)

[41] Plimpton S. Fast parallel algorithms for short-range molecular dynamics. *J Comput Phys* **117**(1): 1–19 (1995)

[42] Mendelev M I, Kramer M J, Ott R T, Sordelet D J, Yagodin D, Popel P. Development of suitable interatomic potentials for simulation of liquid and amorphous Cu–Zr alloys. *Philos Mag* **89**(11): 967–987 (2009)

[43] Jian W R, Long X J, Tang M X, Cai Y, Yao X H, Luo S N. Deformation and spallation of shock-loaded graphene: Effects of orientation and grain boundary. *Carbon* **132**: 520–528 (2018)

[44] Xie Z C, Jian W R, Wang Z H, Zhang X Q, Yao X H. Layer thickness effects on the strengthening and toughening mechanisms in metallic glass–graphene nanolaminates. *Comput Mater Sci* **177**: 109536 (2020)

[45] Tang X C, Meng L Y, Zhan J M, Jian W R, Li W H, Yao X H, Han Y L. Strengthening effects of encapsulating graphene in SiC particle-reinforced Al-matrix composites. *Comput Mater Sci* **153**: 275–281 (2018)

[46] Avila K E, Küchemann S, Alabd Alhafez I, Urbassek H M. Nanoscratching of metallic glasses—An atomistic study. *Tribol Int* **139**: 1–11 (2019)

[47] Jang J I, Yoo B G, Kim Y J, Oh J H, Choi I C, Bei H B. Indentation size effect in bulk metallic glass. *Scripta Mater* **64**(8): 753–756 (2011)

[48] Zhou Q, Wang F, Huang P, Xu K W. Strain rate sensitivity and related plastic deformation mechanism transition in nanoscale Ag/W multilayers. *Thin Solid Films* **571**: 253–259 (2014)

[49] Zhao T Q, Song H Y, An M R, Xiao M X. Effect of graphene on the mechanical properties of metallic glasses: Insight from molecular dynamics simulation. *Mater Chem Phys* **278**: 125695 (2022)

[50] Xu N, Han W Z, Wang Y C, Li J, Shan Z W. Nanoscratching of copper surface by CeO_2. *Acta Mater* **124**: 343–350 (2017)

[51] Yong L, Zhu Y T, Luo X K, Liu Z M. Wear behavior of a Zr-based bulk metallic glass and its composites. *J Alloys Compd* **503**(1): 138–144 (2010)

[52] Fang T H, Liu C H, Shen S T, Prior S D, Ji L W, Wu J H. Nanoscratch behavior of multi-layered films using molecular dynamics. *Appl Phys A* **90**(4): 753–758 (2008)

[53] Wang W Y, Gan B, Lin D Y, Wang J, Wang Y G, Tang B, Kou H C, Shang S L, Wang Y, Gao X Y, et al. High-throughput investigations of configurational-transformation-dominated serrations in CuZr/Cu nanolaminates. *J Mater Sci Technol* **53**: 192–199 (2020)

[54] Wang Z N, Li J, Fang Q H, Liu B, Zhang L C. Investigation into nanoscratching mechanical response of AlCrCuFeNi high-entropy alloys using atomic simulations. *Appl Surf Sci* **416**: 470–481 (2017)

[55] Han D X, Wang G, Ren J L, Yu L P, Yi J, Hussain I, Song S X, Xu H, Chan K C, Liaw P K. Stick–slip dynamics in a $Ni_{62}Nb_{38}$ metallic glass film during nanoscratching. *Acta Mater* **136**: 49–60 (2017)

[56] Zhong C, Zhang H, Cao Q P, Wang X D, Zhang D X, Ramamurty U, Jiang J Z. On the critical thickness for non-localized to localized plastic flow transition in metallic glasses: A molecular dynamics study. *Scripta Mater* **114**: 93–97 (2016)

[57] Hua D P, Ye W T, Jia Q, Zhou Q, Xia Q S, Shi J Q, Deng Y Y, Wang H F. Molecular dynamics simulation of nanoindentation on amorphous/amorphous nanolaminates. *Appl Surf Sci* **511**: 145545 (2020)

[58] Adjaoud O, Albe K. Microstructure formation of metallic nanoglasses: Insights from molecular dynamics simulations. *Acta Mater* **145**: 322–330 (2018)

[59] Lafaye S, Troyon M. On the friction behaviour in nanoscratch testing. *Wear* **261**(7–8): 905–913 (2006)

[60] Lafaye S, Gauthier C, Schirrer R. The ploughing friction: Analytical model with elastic recovery for a conical tip with a blunted spherical extremity. *Tribol Lett* **21**(2): 95–99 (2006)

[61] Mishra M, Szlufarska I. Analytical model for plowing friction at nanoscale. *Tribol Lett* **45**(3): 417–426 (2012)

[62] Xie Y, Hawthorne H M. On the possibility of evaluating the resistance of materials to wear by ploughing using a scratch method. *Wear* **240**(1–2): 65–71 (2000)

[63] Wu Y X, Luo Q, Jiao J, Wei X S, Shen J. Investigating the wear behavior of Fe-based amorphous coatings under nanoscratch tests. *Metals* **7**(4): 118 (2017)

[64] Nasim M, Li Y C, Wen M, Wen C E. High-strength Ni/Al nanolaminates fabricated by magnetron sputtering and their nanoindentation and nanowear behaviors. *Materialia* **6**: 100263 (2019)

[65] Beake B D, Liskiewicz T W. Comparison of nano-fretting and nano-scratch tests on biomedical materials. *Tribol Int* **63**: 123–131 (2013)

[66] Zhang J, Xu Q, Gao L, Ma T B, Qiu M, Hu Y Z, Wang H, Luo J B. A molecular dynamics study of lubricating mechanism of graphene nanoflakes embedded in Cu-based nanocomposite. *Appl Surf Sci* **511**: 145620 (2020)

[67] Kim K S, Lee H J, Lee C G, Lee S K, Jang H, Ahn J H, Kim J H, Lee H J. Chemical vapor deposition-grown graphene: The thinnest solid lubricant. *ACS Nano* **5**(6): 5107–5114 (2011)

Qing ZHOU. He received his Ph.D. degree in material science and engineering from Xi'an Jiaotong University, China, in 2017. After that, he has worked at Northwestern Polytechnical University, China, as an associate professor. From 2021, he worked at Karlsruhe Institute of Technology (KIT, Germany) as a post-doctor. His research areas cover design, fabrication, and characterization of high-performance alloy materials, modeling and simulation of tribological behavior of metal composites, etc.

Shuo LI. He received his Ph.D. degree in mechanics from Xi'an Jiaotong University, China, in 2020. He is currently a post-doctor at the Center of Advanced Lubrication and Seal Materials, State Key Laboratory of Solidification Processing, Northwestern Polytechnical University, China. His research interests include the self-lubricating metallic glass-based composites, molecular dynamics simulation, etc.

Ziqiang CHEN. He received his Ph.D. degree from Xi'an Jiaotong University, China, in 2017. He is now a post-doctor at Institute of Physics, Chinese Academy of Sciences, China, with Professor Weihua WANG. He works as an assistant professor in the College of Engineering and Applied Sciences, Nanjing university, China. His research interests are the correlation between structure and mechanical properties of amorphous alloys and their composites.

Haifeng WANG. He received his Ph.D. degree in material processing engineering from Northwestern Polytechnical University, China, in 2010. He joined the State Key Laboratory of Solidification Processing from 2010 and the Center of Advanced Lubrication and Seal Materials from 2017, at Northwestern Polytechnical University. He worked as a fellow of Alexander von Humboldt Foundation, Germany, during 2011–2013, and a visiting scholar during 2014–2015 in Institut für Materialphysik im Weltraum at Deutsches Zentrum für Luft-und Raumfahrt, Germany. His research areas cover metal-based and ceramic-based wear resistance and lubrication materials, non-equilibrium theory of solidification and solid-state phase-transformation, preparation of non-equilibrium materials including bulk metallic glass and its composite, etc.